Anisotropy in cubic math xmlns="http://www.w3.org/1998/Math/MathML">msub>mi >UO/mi>mn>2/mn>/msub>/math> caused by electron-lattice interactions

Luigi Paolasini, Daniel Chaney, Alexei Bosak, Gerard H. Lander, and Roberto Caciuffo

Phys. Rev. B **104**, 024305 — Published 21 July 2021

DOI: 10.1103/PhysRevB.104.024305

Anisotropy in cubic UO_2 caused by electronic-lattice interactions

Luigi Paolasini,[1] Daniel Chaney,[1,2] Alexei Bosak,[1] Gerard H. Lander,[3] and Roberto Caciuffo[3]

[1]*ESRF, 71 avenue des Martyrs, CS 40220, 38043 Grenoble Cédex 9, France*
[2]*H. H. Wills Physics Laboratory, University of Bristol, Tyndall Avenue, Bristol, BS8 1TL, United Kingdom*
[3]*European Commission, Joint Research Centre, Postfach 2340, D-76125 Karlsruhe, Germany*

(Dated: July 7, 2021)

Despite many years of research, the full complexity of the electronic-lattice interactions in UO_2 is not fully understood. We present X-ray inelastic scattering at low temperature showing that the interaction between electronic degrees of freedom and transverse acoustic phonons is strong only along the reciprocal space direction [100]. The anisotropy is reflected in the phonon-linewidth broadening, which persists also well above the Néel temperature. This intrinsic effect infers an anisotropy in the thermal conductivity, which has been observed, but which is formally forbidden in a cubic material. We have no model capable of connecting our experimental observations with the low thermal conductivity of UO_2 below room temperature.

PACS numbers:

I. INTRODUCTION

Since UO_2 is the world's primary nuclear fuel, the high-temperature (T >1000 K) thermal conductivity has been studied in considerable detail. The phonon dispersions and density-of-states, as well as the phonon lifetimes (which are inversely proportional to the thermal conductivity) have been measured by neutron scattering at several elevated temperatures[1–4]. At the same time UO_2 is also recognized as a complicated small-gap semiconductor (or Mott insulator) with strong interactions at low temperature between the electronic and lattice degrees of freedom, which was first discovered in the 1960's, and still not completely understood; again, this has been extensively studied with scattering (and other) techniques[5–12].

The present paper attempts to build a bridge between these two efforts, and studies the phonon line-widths as a function of temperature over the range 20 to 300 K. As shown by Pang et al. Ref.[2,3], the thermal conductivity is directly related to the phonon line-widths and the dispersion curve, so we are with these measurements probing, albeit indirectly, the thermal conductivity (κ).

Below room temperature the thermal conductivities of ThO_2 and UO_2 are surprisingly different, a fact known for many years[13] despite both materials having the same fluorite structure, and almost identical lattice parameters and phonon dispersion curves[14,15].

The fundamental difference is that there are no $5f$ electrons in ThO_2, but two associated with the uranium ion in UO_2, which orders antiferromagnetically at $T_N = 31$ K. The differences in κ below 300 K between ThO_2 and UO_2 must be driven by electronic-lattice interactions in UO_2, which do not exist in ThO_2. In addition, a recent work[17] has reported that κ of UO_2 is anisotropic over a similar temperature range, and that the value in the $\langle 100 \rangle$ direction is $\approx$10% below that in the two other principal directions.

A number of earlier studies[8,13,18,19] have reported measurements showing that electronic effects in UO_2 extend considerably beyond T_N, suggesting that such interactions could be responsible for the suppression of the thermal conductivity in UO_2 at temperatures below room temperature. To clarify this issue, we need measurements of the phonon lifetimes and their dispersion, as a function of temperature below 300 K. To obtain such information we have used inelastic X-ray scattering (IXS), where a resolution of 1.4 meV is available at high momentum transfer (Q), since the resolution is decoupled from Q[20]. Furthermore, IXS is insensitive to the purely *magnetic* vibrations and direct *quadrupolar* interactions[10,11,21], and measures only the indirect influence of such effects on the lattice vibrations.

II. EXPERIMENTAL DETAILS

The experiments have been performed at the ID28 beamline of the European Synchrotron Radiation Facility (ESRF) on two different quality samples (see Fig.1), using two configurations (technical information can be found in Ref.[20]). For the sample #1 a Si(9,9,9) monochromator configuration was chosen that select an incoming energy E= 17.794 keV, with an instrumental resolution ΔE=3.0 meV. For the sample #2 a higher resolution configuration with a Si(12,12,12) was set at E= 23.725 keV and a resolution of ΔE=1.39(2) meV. All phonons were measured in reflection geometry.

A comparison of the different sample quality can be observed in Fig.2, which shows the room temperature energy scans at (6,0.4,0). The scans of the sample #1 with a good mosaic show a very small contribution of the elastic line, and the phonons groups (Stokes and anti-Stokes) are well defined. The phonon linewidths are resolution limited at room temperature. Both samples gave transverse acoustic (TA) and longitudinal acoustic (LA) phonon energies identical to those well recognised for UO_2, and showed magnetic ordering at $T_N = 31$ K. Finally, in the

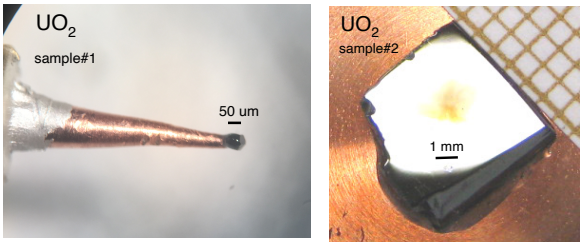

FIG. 1: UO_2 single crystals used for experiments at low resolution ΔE=3 meV (sample #1), and at high resolution ΔE=1.4 meV (sample #2). The latter sample is a large [001]-oriented crystal, with a mosaic of 0.05 degrees, used for earlier studies of the surface magnetism of UO_2[22].

scans on sample #2 with high resolution (ΔE=1.4 meV) the elastic contribution is nearly absent. The incident energy is 23.725 keV, which is above the uranium L_2 edge at 20.948 keV. The 1/e attenuation length (for the beam at 90° incidence) for UO_2 at this energy is $\approx$13.5 μm, so this is not a surface sensitive measurement.

We recall that the intensities of the phonons are governed by Bose-Einstein statistics, so that on cooling from room temperature to 20 K the intensity of the the energy-gain phonon (Stokes, photon energy loss) at +7 meV in Fig.2 decrease by a factor of 4, and the energy-loss phonon (anti-Stokes, photon energy gain) at -7 meV will decrease by a factor of 184. This substantially increases the difficulty of the determining line-widths in the low temperature experiments.

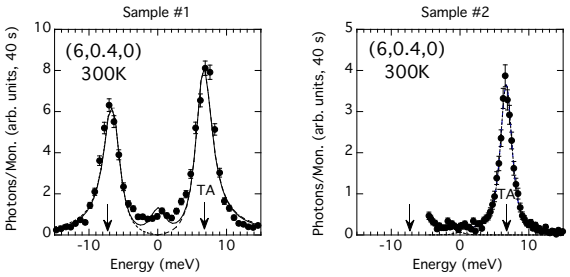

FIG. 2: Comparison of the inelastic TA[100] scans taken at room temperature at (6,0.4,0) for different samples. Sample #1 (left panel) : High quality sample with a good mosaic. The elastic line is nearly absent and the phonon groups are well defined. Sample #2 (right panel): High resolution scans (ΔE=1.4 meV) on the large size and high quality crystal.

III. LOW RESOLUTION EXPERIMENTS

Low resolution experiments were performed on sample #1 and the analysis of the scans collected along the (6k0) Brillouin zone at different temperatures are represented in Fig.3.

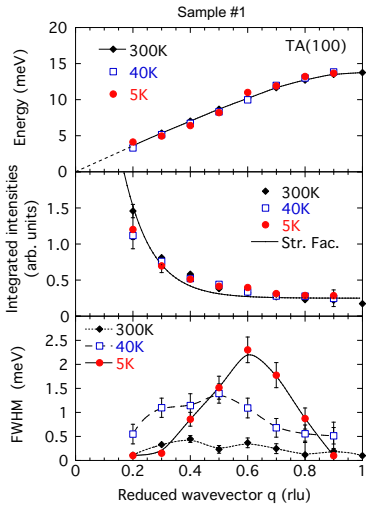

FIG. 3: Analysis of low resolution IXS scans taken across the Brillouin zone (6,k,0) at different temperatures for the samples #1 (Black diamonds 300 K; Blue open square 40 K; red circles 5K). The phonon groups are fit with a single damped harmonic oscillator model de-convoluted with the experimental resolution (Fit28 program, Ref.[20]). Top panel: TA[100] dispersion curve. Middle panel: Integrated phonon intensities normalised with the Bose factor. The line represent the inelastic structure factor calculation. Lower panel: TA(100) phonon linewidth de-convoluted with the experimental resolution.

The TA[100] dispersion curves above the Néel temperature are in agreement with the previous dispersions determined by neutron scattering, and the integrated intensities normalised with the Bose factor follows the predicted theoretical calculation. The experimental resolution of ΔE=3 meV limits the deconvolution of multiple branches appearing below T_N in the anti-crossing regions, however some information exists in the fit results. Using a single damped harmonic oscillator deconvoluted with the experimental resolution, it is possible to extract the phonon linewidth, the FWHM, which is directly related with the inverse of the phonon lifetime. At 5K a large broadening of the TA[100] branch is present in the middle of the Brillouin zone, with the maximum close to the q=0.6 rlu, where the TA[100] phonon interacts with the magnetic excitations. The broadening is present well above T_N, and extends over the entire [100] Brillouin zone. As we will show below, the large broadening of the [100] branch around q = 0.6 rlu is actually due to the splitting of the phonon branches around an avoided crossing, which is unresolved in the low-resolution scans.

IV. HIGH RESOLUTION EXPERIMENTS.

High quality data have been taken using the sample #2 with at E= 23.725 keV, and the complete set of scans

(6,k,0) taken at T=20K across the [100] Brillouin zone. The TA phonons show a resolution limited line-width from the Γ point to q=0.3 rlu, and at q=0.4 rlu a shoulder appears in the high-energy side, as shown in Fig.4. The interacting region between q=0.5 rlu and q=0.7 rlu shows three well defined peaks and Above q=0.8 rlu, up to the zone boundary, the TA phonon becomes again resolution dependent. The fits are done taking into account the instrumental resolution and using a damped harmonic oscillator corrected by the Bose-Einstein thermal population factor. The fit results are presented in the Tab.I for T=20K, and in Tab.II for T larger than T_N.

TABLE I: Transverse acoustic phonon energies E(T) and linewidths Γ(T) in [meV] along the symmetry direction [100] at T=20K for the different vibrational branches (A-B-C). The numbers in parentheses refer to standard deviations on the least-significant digit.

TA [100]						
q	E(20K)-A	Γ(20K)-A	E(20K)-B	Γ(20K)-B	E(20K)-C	Γ(20K)-C
0.1	1.78 (2)	0.18 (7)	-	-	-	-
0.2	3.32 (4)	0.18 (6)	-	-	-	-
0.3	4.98 (2)	0.035 (6)	-	-	-	-
0.4	6.192 (2)	0.011 (6)	7.49 (22)	1.00 (20)		
0.5	6.67 (59)	1.2 (6)	8.12 (1)	0.61 (32)	11.38 (27)	1.42 (57)
0.6	5.54 (23)	1.22 (72)	9.26 (6)	0.47 (18)	12.08 (14)	1.96 (26)
0.7	-	-	10.38 (54)	2.62 (80)	12.49 (19)	1.08 (48)
0.8	-	-	10.59 (42)	1.24 (53)	13.34 (6)	0.27 (14)
0.9	-	-	10.51 (47)	1.51 (49)	13.81 (7)	0.15 (12)

TABLE II: Transverse acoustic phonon energies E(T) and linewidths Γ(T) in [meV] along the symmetry direction [100] at temperature above T_N. The numbers in parentheses refer to standard deviations on the least-significant digit.

TA [100]						
q	E(40K)	Γ(40K)	E(100K)	Γ(100K)	E(295K)	Γ(295K)
0.1	-	-	-	-	1.58 (1)	0.26 (2)
0.2	3.29 (3)	0.62 (8)	-	-	3.60 (2)	0.15 (3)
0.3	5.11 (6)	1.50 (15)	-	-	5.13 (2)	0.30(5)
0.4	6.82 (8)	2.11 (16)	6.92 (5)	1.13 (11)	6.80 (8)	0.42 (6)
0.5	8.52 (7)	2.32 (19)	8.70 (7)	1.24 (18)	8.43 (5)	0.43 (9)
0.6	10.35 (7)	2.04 (22)	10.25 (7)	0.68 (15)	9.64 (18)	0.31 (10)
0.7	11.72 (6)	1.21 (16)	11.75 (6)	0.45 (16)	10.74 (15)	0.32 (10)
0.8	-	-	-	-	11.74 (2)	0.02 (1)
0.9	-	-	-	-	13.52 (2)	0.04 (3)

Fig.4 shows the data obtained below T_N and the quality can be compared directly to the best neutron data reported in Ref.[12].

All scans in Fig.4 show finite intensity at E = 0 position. This quasi-elastic scattering (which is resolution limited in energy) is not present at T = 300 K, as shown by the clean scans in right-hand panel of Fig.2-A. A further discussion of this scattering will be given later.

The dispersion curves in the [100] and [011] directions are shown in Fig.5 and are color coded to enable the different branches to be identified. In the [100] direction there are two main regions of interaction between the vibrational and electronic degrees of freedom. The first is around q = 0.45 rlu and has long been known to be important[5,6], as it occurs between the TA[100] phonon and the acoustic magnon branch that has its minimum at the X-point (q = 1.0 rlu) with a gap of ≈2 meV (branches A-B).

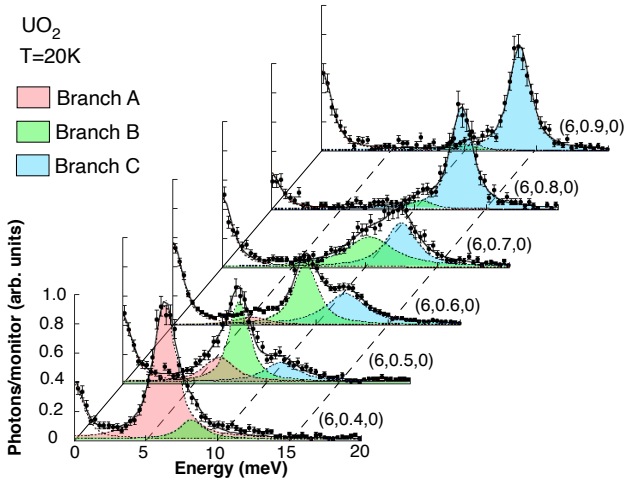

FIG. 4: Inelastic x-ray scattering scans taken at 20 K across the (6,q,0) Brillouin zone. The transverse acoustic phonon TA[100] shows anti-crossings that correspond to the two regions at q=0.45 rlu with the acoustic magnon mode and at q=0.65 rlu with the optic magnon mode. The color coding identifies branches on the dispersion curves of Fig.5.

The second is around q = 0.65 rlu (branches B-C), and has not been previously observed, although anti-crossings are predicted in this region of the Brillouin zone[11]. The reason why this phonon interaction between energies of approximately 9 to 12 meV was not previously observed in neutron scattering is that at these energies there is a strong signal from the mixed optic magnon-quadrupolar mode[12], making it difficult (even with polarized neutrons) to separate the complex signals. With x-rays this is much simpler as purely magnetic or quadrupolar modes cannot be observed, the technique being sensitive only to the vibrational component of the mixed modes.

The dispersion of branch (C) is in good agreement with the theoretical calculations[11], and is associated with the interaction of the TA[100] phonon with the optic magnon and quadrupolar modes (both acoustic and optic). The branch (B) associated with this anti-crossing appears to be shifted to higher energy (∼1meV) with respect to the neutron results. However, as discussed below, these TA branches show strong line broadening over this range of q, so that the exact frequency is hard to establish.

The strong interaction at these energies has also been observed in recent density-of-states measurements using neutrons and polycrystalline samples (see Fig. 2 of Ref. [4]). This figure shows strong scattering in this energy range out to Q values much higher than expected for purely magnetic scattering, where the magnetic form factor of U^{4+} would not anticipate intensity for Q values above ∼ 6 $Å^{-1}$ (see Ref.[7]). However, these measurements cannot determine where in the Brillouin zone these interactions occur, as polycrystalline samples were used.

The comparison of the temperature dependence of the

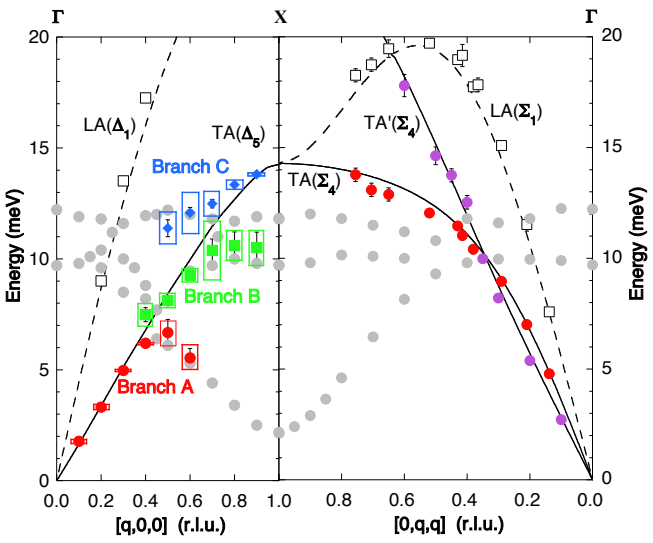

FIG. 5: Dispersion curves measured at T=20K with inelastic x-ray scattering of transverse (color filled symbols, TA) and longitudinal (open squares, LA) acoustic phonons in the [100] and [011] reciprocal lattice directions. The solid (dashed) lines represent the transverse (longitudinal) acoustic phonon branches calculated at room temperature. The dispersion of the magnetic excitations, determined by neutron inelastic scattering, are also indicated (gray dots)[12]. The TA(Δ_5) phonon branch splits into three branches (A), (B) and (C) as a result of the interactions with the acoustic magnon branch (A), and with the optic magnon branches (B) and (C). No interactions involving the TA(Σ_4) or TA'(Σ_4) is observed in the [011] direction. The color-coded rectangles refer to the energy linewidth broadening of the TA[100] branches in correspondence of the anti-crossing regions.

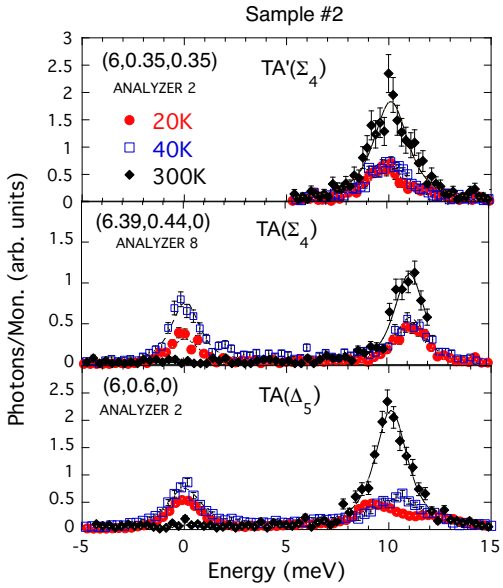

FIG. 6: Comparison of temperature dependence of TA phonons in the [100] and [011] directions. A finite phonon lifetime is clearly observed in the TA[100] at 40K (bottom panel), well above T_N=30.8 K. Below T_N the TA[100] phonon splits in correspondence of the anti-crossing region, as described in the text. The TA'[011] and TA[011] phonons have a linewidth close to the experimental resolution, as shown in the fit results presented in Tab.III and Tab.IV, respectively.

phonon groups between the [100] and the [011] directions is shown in Fig.6. The scans are taken close to the middle of the Brillouin zones where the interaction with the magnetic excitations are expected. The non-degenerate transverse branches TA(Σ_4) and TA'(Σ_4) in the [011] directions can be fitted with a resolution dependent linewidths at all temperatures and over the entire Brillouin zone [011], whereas the TA(Δ_5) in the [100] direction shows the specific broadening due to the anti-crossing with the acoustic and optic magnetic excitations.

These scans also show the signal at E=0, which has a strong T dependence and is not present at 295 K. Other scans (not shown) just over the phonon modes were used to extract the linewidths.

Tab.III and Tab.IV show the results of the fit for the acoustic phonon branches TA'[011] and TA[011], respectively, taken at different temperatures around the interaction energy regions with the magnetic excitations (see Fig.5).

Fig.7 shows the evolution of the FWHM of the TA[100] across the Brillouin zone as a function of temperature. The arrows indicate the anti-crossing positions where the vibrational modes below T_N exchange their characters

TABLE III: Transverse acoustic phonon TA'[011] energies E(T) and linewidths Γ(T) in [meV] along the symmetry direction [011] (analyzer 2, resolution ΔE=1.5 meV). The numbers in parentheses refer to standard deviations on the least-significant digit.

TA' [011] (H,K,L)	E(20K)	Γ(20K)	E(40K)	Γ(40K)	E(300K)	Γ(300K)
(6,0.2,0.2)	5.47 (14)	0.31 (12)	5.56 (7)	0.66 (13)	5.38 (4)	0.30 (7)
(6,0.3,0.3)	8.00 (9)	0.32 (19)	-	-	8.21 (20)	0.29 (11)
(6,0.35,0.35)	9.84 (8)	0.60 (24)	9.42 (12)	0.86 (20)	9.98 (2)	0.48 (4)
(6,0.4,0.4)	12.11 (2)	1.03 (4)	12.17 (7)	0.42 (17)	12.53 (8)	0.44 (20)
(6,0.45,0.45)	13.31 (12)	0.88 (23)	-	-	13.75 (6)	0.13 (8)

TABLE IV: Transverse acoustic phonon TA[011] energies E(T) and linewidths Γ(T) in [meV] along the symmetry direction [011] (resolution ΔE=1.5 meV). The analyzer number is also indicated. The numbers in parentheses refer to standard deviations on the least-significant digit.

TA [011] (H,K,L)	Anal.	E(20K)	Γ(20K)	E(40K)	Γ(40K)	E(300K)	Γ(300K)
(6.13,0.14,0)	7	4.79 (7)	0.65 (2)	-	-	4.59 (9)	0.47 (15)
(6.39,0.44,0)	8	11.04 (1)	0.02 (3)	11.03 (1)	0.07 (2)	11.00 (6)	0.10 (15)
(6.64,0.66,0)	9	12.89 (8)	0.48 (19)	13.08 (9)	0.81 (27)	12.80 (7)	0.46 (20)
(6.64,0.77,0)	9	13.10 (1)	0.21 (12)	13.14 (2)	0.06 (1)	12.98 (1)	0.08 (11)

(magnon-like or phonon-like).

In the [011] direction, in strong contrast to the above complex situation in the [100] direction, we have detected no interactions between the vibrational and electronic systems. The theory published in Ref.[11,12] does not address directly the phonon lifetimes, but focuses on the

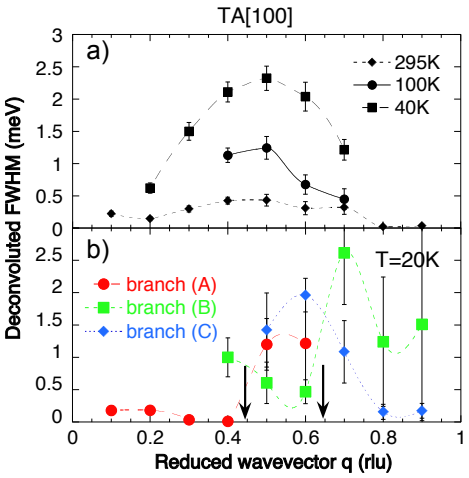

FIG. 7: Temperature dependence of TA[100] phonon linewidth (deconvoluted with the instrumental resolution). The upper panel shows the phonon broadening above T_N, whereas the bottom panel shows the evolution of linewidths of the different phonon branches across the two anti-crossing regions (indicate by arrows), as described in the main text.

presence or absence of anti-crossings. In the [100] direction our experiments show that the anti-crossings are associated with phonon splitting and broadening. However, this does not appear to be the case in the [011] direction, where the theory, calculated in the framework of random phase approximation, predicts several anti-crossings around the position [0 0.5 0.5].

The q-dependence of the linewidth broadening in the [100] direction, shown as rectangles in Fig.5, is fairly small for q<0.4 rlu, but is especially important for branch B and C, and has an overall broad maximum at q $\sim$ 0.6 rlu.

The modes of the TA(Δ_5) are clearly affected, especially in the energy region of 5–15 meV. The largest value of the linewidth broadening is in the ordered state below T_N, but it extends to much higher temperatures, as discussed further below.

At the same time, we have observed a signal that appears quasi-elastic (i.e. at E = 0) at the energy resolution of the experiment, and that is especially strong just above T_N. The momentum dependence of this signal is different from that of the phonon linewidth broadening; it occurs at all wave-vectors examined and, unlike the linewidth broadening, is not confined to the [100] direction. This quasi-elastic scattering is first shown in Fig.4, where the positive signal at E = 0 with the sample at T = 20 K, should be compared with that in Fig.2 (right hand panel) using the same crystal and resolution at T = 300 K.

We show in Fig.8 the quasi-elastic signal at the position of the TA(Σ_4) with q = 0.2 rlu in the [0 q q] direction, as a function of temperature. Experiments with neutrons have observed this signal but without polarization analysis cannot separate the lattice from the magnetic contributions[8].

V. DISCUSSION AND CONCLUSIONS

In comparing the phonon linewidths with the thermal conductivity, we need to recall that the thermal conductivity $\kappa_{\mathbf{q},j}$ due to phonons with quasi-momentum $\mathbf{q}$ and belonging to the branch j is given by:

$$\kappa_{\mathbf{q},j} = \frac{1}{3} C_{\mathbf{q},j} v^2_{\mathbf{q},j} / \Gamma_{\mathbf{q},j} \qquad (1)$$

where $C_{\mathbf{q},j}$ is the phonon heat capacity and $v_{\mathbf{q},j} = \delta E_{\mathbf{q},j}/\delta \mathbf{q}$ is the group velocity determined by the local dispersion gradient. The phonon mean free path $\lambda_{\mathbf{q},j} = v_{\mathbf{q},j}\tau_{\mathbf{q},j}$ depends on the measured phonon linewidth through the relaxation time $\tau_{\mathbf{q},j} = 1/\Gamma_{\mathbf{q},j}$. *Since there are no conduction electrons in UO_2, there is a direct link between the lifetime of the phonons, and the thermal conductivity, as discussed in Ref.[2,3].*

We are not able to calculate the total thermal conductivity as a function of temperature, as we do not have any measure of the optic modes. Such measurements are almost impossible with IXS, as the optic modes predominantly reflect the motion of oxygen atoms[2–4,23] and for these modes the X-ray cross section is very small.

However, below 150 K the primary contributors to the thermal conductivity are the acoustic modes. This is because the low thermal population of the optics modes (whose energy has a minimum of 20 meV for the LO_1 branch at the X point of the Brillouin zone). Our results show that at low temperatures (up to at least 200 K) the phonon line-widths in UO_2 are broadened a significant amount, and that the values steadily decrease as the temperature is raised from the base value. This is shown schematically in Fig.8 by the solid squares and the dotted line joining them. At the same time, these values of the line-widths are anisotropic, they clearly exist in the [100] direction, but we have failed to detect any significant effect in the [011] direction. The linewidth broadening has essentially disappeared at higher temperatures, and our (small) phonon linewidths at 300 K are therefore in good agreement with the measurements and calculations of Pang et al.[2,3].

In practical terms the linewidth broadening then increases again above room temperature and has been carefully characterized experimentally (and theoretically) by Pang et al. [2,3]. This results in a degradation of the thermal conductivity at higher temperature, which together with the effect of radiation damage, has important consequences for reactor operations. We might therefore ask the question as to whether the linewidth broadening at lower temperatures in UO_2 also reduces the thermal conductivity. Presently, we have no model to understand the electronic-lattice interactions in UO_2 at low temperature, nor the anisotropy we have observed, so caution is

necessary in making a connection between the bulk measurements of Ref.[17] and our microscopic measurements. There is clearly a difference in the temperature dependence, but we note that the primary effect in the measurements of Ref.[17] is along the [100] direction, which is consistent with our observations.

Since the thermal conductivity should be isotropic in a cubic material, we emphasize that this condition requires that the perturbation of the phonon spectra does not break the cubic symmetry. Neither ordered dipole magnetism nor pure phonon-phonon interactions can change this symmetry requirement. However, electronic-lattice interactions, such as we observe in UO_2, together with the associated correlation effects, may lead to anisotropic effects in the thermal conductivity. They do not, however, necessarily require a distortion of the overall unit cell, and indeed none has been observed in UO_2. The quadrupoles induce an internal distortion of the oxygen atoms, which leads to a reduction in the symmetry from $Fm\bar{3}m$ to $Pa\bar{3}$, but it remains cubic, at least at the global symmetry level[7,10].

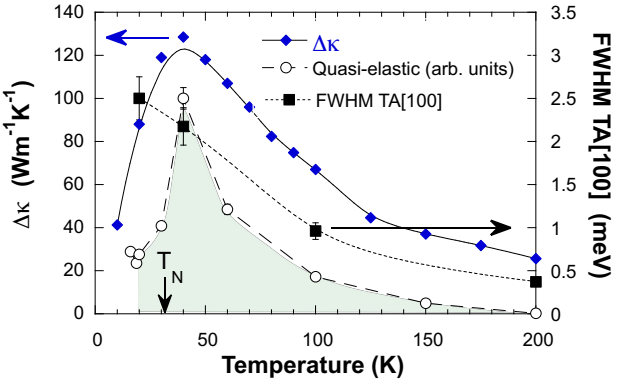

FIG. 8: Comparison of temperature dependence between the thermal conductivity difference $\Delta\kappa = \kappa(ThO_2) - \kappa(UO_2)$ (filled diamond symbols)[13,16], the FWHM of TA[100] averaged over values at the center of the zone (black filled squares), and the normalised quasi-elastic integrated intensities (open circles, shaded area). Lines are guide for the eyes.

Finally, our measurements have observed a quasi-elastic contribution (Fig.8) to the scattering that appears to have a peak intensity just above T_N and be present at all momentum transfers examined, i.e. it is not seen only along the [100] direction, as is the linewidth broadening. The temperature dependence is also different from the linewidth broadening (Fig.8), with a peak just above T_N. Unlike the signal from the disordered magnetic moments, this incoherent signal is clearly present also below T_N, so may be related to the local breaking of the apparent cubic global symmetry. Although further experiments are necessary, this signal resembles the polaron-like behavior found in the manganites exhibiting colossal magnetoresistance[24–27]. Such polarons could arise from coupling of the quadrupoles and their local oxygen distortions to the lattice, causing dynamical strain effects that would be observed at all wave-vectors indicating uncorrelated lattice deformations. Further experiments (and theory) will clearly have to be performed on this aspect.

Unlike in the case of the manganites, there is no structural transition in UO_2 reducing the symmetry from cubic below T_N[9,10], so a more subtle origin of any possible polarons is required. In this case, they could arise from strain induced by the disordered quadrupoles and the consequent local shifts of the oxygen atoms[7,9], as the effect is maximum just above T_N (see Fig.8). Such interactions in UO_2 could play a key role in the line broadening of the phonons.

Recent theoretical advances in modelling the thermal conductivity[28,29] and understanding[30–35] the complex electronic state of actinide dioxides at low temperatures gives hope that the measurements reported in this paper will spur additional theoretical efforts.

Acknowledgments

We thank Chris Stanek and David Andersson of Los Alamos National Laboratory for useful discussions. We thank Myron Huzan for his help on the analysis of low resolution data during his stage at ILL/ESRF Summer School Program. We thank Denis Gambetti for his technical help at ID28-ESRF beamline.

[1] K. Clausen, W. Hayes, J. E. McDonald, R. Osborn, and M. T. Hutchings, Phys. Rev. Lett. **52**, 1238 (1984).
[2] J. W. L. Pang, W. J. L. Buyers, A. Chernatynskiy, M. D. Lumsden, B. C. Larson, and S. R. Phillpot, Phys. Rev. Lett. **110**, 157401 (2013).
[3] J. W. L. Pang, A. Chernatynskiy, B. C. Larson, W. J. L. Buyers, D. L. Abernathy, K. J. McClellan, and S. R. Phillpot, Phys. Rev. B **89**, 115132 (2014).
[4] M. S. Bryan, J. W. L. Pang, B. C. Larson, A. Chernatynskiy, D. L. Abernathy, K. Gofryk, and M. E. Manley. Phys. Rev. Materials **3**, 065405, (2019).
[5] G. Dolling and R. A. Cowley, Phys. Rev. Lett., **16**, 683 (1966).
[6] R. A. Cowley and G. Dolling, Phys. Rev. 16**7** 464 (1968).
[7] J. Faber and G. H. Lander, Phys. Rev. B **14**, 1151 (1976).
[8] R. Caciuffo, G. Amoretti, P. Santini, G. H. Lander, J. Kulda, and P. de V. Du Plessis, Phys. Rev. B **59**, 13892 (1999).
[9] S.B. Wilkins, R. Caciuffo, C. Detlefs, J. Rebizant, E. Colineau, F. Wastin, and G.H. Lander, Phys. Rev. B **73**, 060406(R) (2006).
[10] P. Santini, S. Carretta, G. Amoretti, R. Caciuffo, N. Mag-

nani, and G. H. Lander, Rev. Mod. Phys. **81**, 807 (2009).
[11] S. Carretta, P. Santini, R. Caciuffo, and G. Amoretti, Phys. Rev. Lett., 105, 167201 (2010); *ibid:* Supplementary online material.
[12] R. Caciuffo, P. Santini, S. Carretta, G. Amoretti, A. Hiess, N. Magnani, L.-P. Regnault, and G. H. Lander, Phys. Rev. B **84**, 104409 (2011).
[13] J. P. Moore & D. L. McElroy, J. American Ceramic Soc. **54**, 40 (1971). This work shows that the thermal conductivity of UO_2 does not depend on the form of the material.
[14] K. Clausen, W. Hayes, J. E. Macdonald, R. Osborn, P. G. Schnabel, M. T. Hutchings, and A. Magerl, J. Chem. Soc., Faraday Trans. 2, **83**, 1109 (1987).
[15] Y. Lu, Y. Yang, and P. Zhang, J. Phys.: Cond. Matt. **24** 225801 (2012).
[16] M. Mann, D. Thompson, K. Serivalsatit, T. M. Tritt, J. Ballato, and J. Kolis, Cryst. Growth and Design **10**, 2146 (2010).
[17] K. Gofryk, S. Du, C. R. Stanek, J.C. Lashley, X.-Y. Liu, R.K. Schulze, J. L. Smith, D. J. Safarik, D. D. Byler, K. J. McClellan, B. P. Uberuaga, B. L. Scott and D. A. Andersson, Nat. Comm. **5**, 4551 (2014).
[18] O. G. Brandt and C. T. Walker, Phys. Rev. **170**, 528 (1968).
[19] K. Sasaki and Y. Obata, J. Phys. Soc. Japan **28**, 1157 (1970).
[20] Beamline description can be found at web site *https://www.esrf.eu/home/UsersAndScience/Experiments/EMD/ID28.html*.
[21] The x-ray energies used for phonon experiments are determined by the plane spacings of the Si monochromator used in the instrument and are far removed from the resonant energies used for observing the quadrupole effects reported in Ref.[9,10].
[22] G. M. Watson, Doon Gibbs, G. H. Lander, B. D. Gaulin, L. E. Berman, Hj. Matzke, and W. Ellis, Phys. Rev. Lett. **77**, 751 (1996).
[23] S. Rennie, E. Lawrence Bright, J. E. Darnbrough, L. Paolasini, A. Bosak, A. D. Smith, N. Mason, G. H. Lander, and R. Springell, Phys. Rev. B **97**, 224303 (2018).
[24] S. Shimomura, N. Wakabayashi, H. Kuwahara, and Y. Tokura, Phys. Rev. Lett. **83**, 4389 (1999).
[25] L. Vasiliu-Doloc, S. Rosenkranz, R. Osborn, S. K. Sinha, J. W. Lynn, J. Mesot, O. H. Seeck, G. Preosti, A. J. Fedro, and J. F. Mitchell, Phys. Rev. Lett. **83**, 4393 (1999).
[26] F. Weber, N. Aliouane, H. Zheng, J. F. Mitchell, D. N. Argyriou, and D. Reznik, Nat. Mat. **8**, 798 (2009).
[27] M. Maschek, D. Lamago, J-P. Castellan, A. Bosak, D. Reznik, and F. Weber, Phys. Rev. B **93**, 045112 (2016).
[28] Miaomiao Jin, Marat Khazov, Chao Jiang, Shuxiang Zhou, Chris A., Marianetti, Matthew S. Bryan, Michael E. Manley, and David H. Hurley, J. of Phys.: Cond. Matter, **33** 275402 (2021).
[29] Hiroki Nakamura, Masahiko Machida, Journal of Nuclear Materials **519** 45 (2019).
[30] Jindřich Kolorenč,Alexander B. Shick, and Alexander I. Lichtenstein, Physical Review B **92**, 085125 (2015).
[31] Li Huang, Yilin Wang and Philipp Werner, EPL **119** 57007 (2017).
[32] Nicola Lanatá, Yongxin Yao, Xiaoyu Deng, Vladimir Dobrosavljević, and Gabriel Kotliar, Phys. Rev. Lett. **118**, 126401 (2017)
[33] S. L. Dudarev, P. Liu, D. A. Andersson, C. R. Stanek, T. Ozaki, and C. Franchini, Physical Review Materials **3**, 083802 (2019).
[34] Leonid V. Pourovskii and Sergii Khmelevskyic, Phys. Rev. B **99**, 094439 (2019).
[35] Leonid V. Pourovskii and Sergii Khmelevskyic, PNAS Vol. **118** No. 14 e2025317118 (2021).